Author Manuscript

Author Manuscript

Author Manuscript

Author Manuscript

HHS Public Access

Author manuscript

Eur J Immunol. Author manuscript; available in PMC 2024 June 13.

Published in final edited form as:

Eur J Immunol. 2018 July ; 48(7): 1174–1180. doi:10.1002/eji.201847480.

NCR+ ILC3 maintain larger STAT4 reservoir via T-BET to regulate type 1 features upon IL-23 stimulation

Yohei Mikami[1], **Gianluca Scarno**[2], **Beatrice Zitti**[3], **Han-Yu Shih**[1], **Yuka Kanno**[1], **Angela Santoni**[2,4], **John J O'Shea**[1], **Giuseppe Sciumè**[2,*]

[1]Lymphocyte and Cell Biology Section, Molecular Immunology and Inflammation Branch, National Institute of Arthritis and Musculoskeletal and Skin Diseases, NIH, Bethesda, Maryland, USA.

[2]Department of Molecular Medicine, Sapienza University of Rome, Laboratory affiliated to Istituto Pasteur Italia – Fondazione Cenci Bolognetti, Rome, Italy.

[3]HERM, Department of Medicine, Karolinska Institutet, Stockholm, Sweden.

[4]IRCCS Neuromed, 86077, Pozzilli (IS), Italy.

Abstract

Innate lymphoid cells (ILCs) producing IL-22 and/or IL-17, designated as ILC3, comprise a heterogeneous subset of cells involved in regulation of gut barrier homeostasis and inflammation. Exogenous environmental cues in conjunction with regulated expression of endogenous factors are key determinants of plasticity of ILC3 towards the type 1 fate. Herein, by using mouse models and transcriptomic approaches, we defined at the molecular level, initial events driving ILC3 expressing natural cytotoxicity receptors (NCR^+ ILC3) to acquire type 1 features. We observed that NCR^+ ILC3 exhibited high basal expression of the signal-dependent transcription factor STAT4 due to T-BET, leading to predisposed potential for the type 1 response. We found that the prototypical inducer of type 3 response, IL-23, played a predominant role over IL-12 by accessing STAT4 and preferentially inducing its phosphorylation in ILC3 expressing T-BET. The early effector program driven by IL-23 was characterized by the expression of IL-22, followed by a production of IFN-γ, which relies on STAT4, T-BET and required chromatin remodeling of the *Ifng* locus. Altogether, our findings shed light on a feed-forward mechanism involving STAT4 and T-BET that modulates the outcome of IL-23 signaling in ILC3.

Keywords

Innate lymphoid cells; STAT4; IFN-γ; transcriptome; mucosal immunology

[*]Corresponding author: Giuseppe Sciumè, Viale Regina Elena, 291 00161, Rome. Italy. Fax: +39 06 44340632, giuseppe.sciume@uniroma1.it.

[6]Conflict of Interest

The authors declare no commercial or financial conflict of interest.

Author Manuscript Author Manuscript Author Manuscript Author Manuscript

1 Introduction

Lymphocyte specification is controlled by regulated expression of lineage-defining (LDTF) and signal-dependent transcription factors (SDTF). Based on the expression pattern of LDTFs and cytokines, three major groups of innate lymphoid cells can be discriminated[1]. Mirroring the typical traits of distinct T cell subsets, type 1 ILCs comprise natural killer (NK) cells and other interferon-γ (IFN-γ)-producing cells, overall named ILC1, whereas innate lymphocytes producing cytokines associated with T helper 2 response fall into the ILC2 group. Finally, type 3 ILCs (ILC3) are generally characterized by the expression of interleukin (IL)-22 and requirement of the LDTF RORγt[2]. Distinct ILC3 subsets can be further discerned based on the expression of CD4, CCR6 and natural cytotoxicity receptors (NCRs)[3],[4]. Despite their phenotypic similarity with NK cells, NCR^+ ILC3 were initially identified for their ability to produce IL-22, both in human and mouse, and lack of the typical NK cell effector functions[5]–[8]. However, the requirement of the LDTFs of ILC1, T-BET (encoded by *Tbx21*), functionally positions these cells as a bridge between type 1 and type 3 ILCs[9]–[11], and delineates their hybrid transcriptional and epigenetic programs[12],[13].

NCR^+ ILC3 are predominantly located in the lamina propria of the intestine, having both redundant and nonredundant roles in promoting gut inflammation[14],[15]. In this context, SDTFs can shape the effector programs of NCR^+ ILC3. Among them, members of the Signal Transducer and Activator of Transcription (STAT) family play a pivotal role in regulation of ILC functions[16]. Beyond STAT5, which orchestrates the development of all ILCs and has a peculiar requirement in NCR^+ ILC3[17], STAT3 has been demonstrated to be a key regulator of the effector functions of the whole ILC3 compartment, downstream of IL-23 activity[18],[19]. On the other hand, STAT4 has specific roles in regulating NK cells and ILC1 functions; however, the controlled expression of STAT4 is important for determining NK functional output during course of infection[20]–[22].

IL-12 and IL-23, two cytokines that signal via STAT4, have been implicated in the functional plasticity of NCR^+ ILC3 towards the ILC1 phenotype[10],[23]–[25]; however, the mechanistic basis of this phenomenon have not yet been characterized. In this study, through the combination of mouse models and genomic approaches, we assessed the expression of STAT4 in ILC3, the role of T-BET in regulation of its expression and its functional relevance. We observed that expression of T-BET, along with the selective ability of IL-23 to induce both STAT4 activation and epigenetic changes led to distinct effector programs in ILC3. Thus, different ILC3 subsets can have distinct activation outcomes through the coordinated expression of both LDTFs, and regulated expression of SDTFs.

2 Results and Discussion

2.1 NCR^+ ILC3 selectively express high basal levels of STAT4

We began our investigations by examining STAT4 expression in ILC3 subsets under basal conditions. We analyzed $CD3\varepsilon^-ROR\gamma t^+$ cells based on the expression of NKp46 and CD4, and included $ROR\gamma t^-NKp46^+$ cells, which comprise both ILC1 and NK cells, as controls (Fig. 1A and Supporting information Fig. 1A). As shown in Fig. 1B, type 1 ILCs expressed

Author Manuscript Author Manuscript Author Manuscript Author Manuscript

high levels of STAT4, reflecting its previously established role in regulating NK and ILC1 functions. However, STAT4 expression was not restricted to type 1 cells, since we also found high basal levels of this TF in NCR^+ ILC3. In contrast, STAT4 was barely detectable in $CD4^+$ ILC3 (Fig. 1B).

NCR^+ ILC3 originate from a fraction of $CD4^-NCR^-$ ILC3 that express T-BET[11]. Thus, we further analyzed the latter ILC3 population for T-BET expression and STAT4 levels. Notably, we mainly detected STAT4 expression in the fraction of $T\text{-}BET^+$ cells (Fig. 1C), although at lower levels as compared to NCR^+ ILC3 (Fig. 1D). These data indicated that both the LDTF and SDTF leading the type 1 effector programs emerge simultaneously in ILC3. This observation led us to investigate whether T-BET could have a role in regulation of STAT4 expression.

$T\text{-}BET^+$ ILC3 are characterized by the low expression of the chemokine receptor CCR6. The absence of T-BET in $CCR6^-$ ILC3 results in a developmental block, and accumulation of cells in the intestinal lamina propria that lack expression of NCR receptors[10]. As shown in Fig. 1E, $CCR6^-$ ILC3 isolated from *Tbx21*$^{-/-}$ mice lack the high STAT4 expression that is seen in their WT counterparts, indicating T-BET as an inducer of STAT4 expression in this subset of ILCs. The differential STAT4 expression observed in ILC3 was correlated with the presence of regulatory elements specifically accessible in the *Stat4* locus of NCR^+ ILC3 (Supporting information Fig. 1B). In support of the direct role of T-BET underlying STAT4 expression, these specific regulatory elements corresponded to T-BET-binding sites (Supporting information Fig. 1B).

In contrast to ILC3, there was only a trend showing a partial reduction of STAT4 expression in *Tbx21*$^{-/-}$ type 1 ILCs (Supporting information Fig. 1C), arguing for alternative means of regulation in these cells. In this regard, the expression of the other T-BOX family member, EOMES, observed in the NK cells persisting in *Tbx21*$^{-/-}$ mice could compensate for the absence of T-BET[9].

Thus, our data show selective high basal STAT4 expression levels in NCR^+ ILC3, equivalent to that of ILC1, correlating with T-BET expression. Moreover, our findings provide evidence for the requirement of T-BET for maintenance of STAT4 in ILC3 but not ILC1.

2.2 IL-23 drives STAT4 activation in NCR^+ ILC3

IL-23 and IL-12 are most often linked to STAT3 and STAT4 activation, respectively. Many, if not all, cytokines activate multiple STATs and the output of cytokine signaling is modulated by the dynamic regulated expression of different STATs[20],[26]. Moreover, as IL-23 and IL-12 share a receptor subunit, they both have the capacity to induce robust STAT4 phosphorylation[27].

Therefore, we measured the activity of both cytokines in NCR^+ ILC3 and type 1 ILCs, positing that with high basal STAT expression, the typical preferential STAT usage might be altered. As shown in Fig. 2A, IL-23 induced STAT4 phosphorylation in NCR^+ ILC3, along with prominent STAT3 phosphorylation, in contrast to ILC1 in which neither STAT was

Author Manuscript Author Manuscript Author Manuscript Author Manuscript

activated (see also Supporting information Fig. 2A). By contrast, IL-12 activated STAT4, and partially STAT3, only in type 1 ILCs (Figure 2B and Supporting information 2B).

2.3 Divergent and redundant transcriptomic effects of IL-23 in ILC3

To define the potential impact of IL-23 stimulation in cells that manifest differential STAT3 and STAT4 activation, we analyzed the transcriptomes of NCR^+ and $CD4^-NCR^-$ ILC3 acutely treated with this cytokine (Supporting information table 1). In effort to gain further functional insights, we used a stringent cut-off[28] (fold change higher than 4) to identify the most highly IL-23 regulated genes in each population (Supporting information table 2, for complete list of upregulated and downregulated genes). Through this approach, we defined 51 highly induced genes in NCR^+ and 38 in $CD4^-NCR^-$ ILC3. Transcripts encoding for genes typically associated with the type 3 response, such as *Il22, Il1r1, Socs3 and Il17f* were at the top of the two gene lists (Fig. 2C). By analysis of the absolute expression, we identified both specific (cluster 1 and 3) and redundant (cluster 2) activation programs downstream of IL-23 between 2 populations of ILC3 (Fig. 2D, and Supporting information table 3). Genes encoding IL-17 were highly expressed mainly in NCR^- ILC3 (as previously described [29],[30]), whereas *Il22, Il1r1 and Socs3* were expressed at similar levels in both ILC3 populations, after IL-23 stimulation. Finally, in activated NCR^+ ILC3, we observed prominent expression of transcripts previously associated with the NK cell response, such as *Ccr5*, *Gzma, Prdm1* (encoding for BLIMP1) and *Ifitm1* [31]. In contrast to the high expression levels of IL-22, and the induction of NK cell related genes, the eponymous cytokine of the type 1 response, IFN-γ, was not induced either at RNA (Fig. 2C,D) or protein level (Fig. 2E) after this acute stimulation of 4 hours, which led us to further investigate the mechanisms underlying differential regulation of IL-22 and IFN-γ.

2.4 Asymmetric regulation of IL-22 and IFN-γ in NCR^+ ILC3

Despite of the pivotal role of T-BET and the activity of IL-23 in regulation of the homeostatic pool of NCR^+ ILC3 [9]–[11], the deletion of *Stat4* did not affect generation of this subset. Indeed, $Stat4^{-/-}$ mice did not present significant alterations of the ILC3 populations (Fig. 3A). Thus, we capitalized on the preservation of NCR^+ ILC3 in $Stat4^{-/-}$ mice to evaluate the functional role of this TF in regulating IL-22 and IFN-γ expression. After treatment with IL-23, both WT and $Stat4^{-/-}$ NCR^+ ILC3 expressed comparable levels of IL-22 (Fig. 3B), as well, expression of the two LDTFs, T-BET and RORγt was not altered in $Stat4^{-/-}$ mice (Supporting information Fig. 3A). On the other hand, as shown in Fig. 2E, IFN-γ production was not detected at the time when IL-22 was produced in WT cells despite that IL-23 activated both STAT3 and STAT4 (Fig. 2A). To gain further insight into the regulation of IFN-γ, we evaluated chromatin accessibility of the *Ifng* locus, including distal enhancer elements. While resting NCR^+ ILC3 showed limited accessibilities of the *Ifng* locus compared with NK cells, we observed *de novo* appearance of accessible regulatory elements induced by IL-23 treatment (Fig. 3C). This led us to hypothesize that delayed expression of IFN-γ could be occurring. In support of this hypothesis, we observed production of IFN-γ in NCR^+ ILC3 after 8- and 16-hour stimulation with IL-23 (Fig. 3D). In these conditions, NCR^+ ILC3 were the main producer of IFN-γ, not only in the context of ILCs (Fig. 3E and Supporting information Fig. 3B), but also when compared to total $CD3\varepsilon^+$ T cells (Supporting information Fig. 3C). Notably, *Stat4* deletion was associated

Author Manuscript Author Manuscript Author Manuscript Author Manuscript

with a reduced IFN-γ response in NCR^+ ILC3 after IL-23 treatment, while no significant difference was observed in $CD4^-NCR^-$ ILC3 (Fig. 3F). Our observation collectively predicts that NCR^+ ILC3 holds the potential to become not only IL-22 but also IFN-γ producers in response to inflammatory environment and their IFN-γ response is partially through STAT4.

To address the *in vivo* relevance of our findings, we tested a colitis model and evaluated the expression of IFN-γ in ILC3. In these settings, NCR^+ ILC3 still maintained their preferential responsivity to IL-23, over IL-12 (data not shown), and were able to respond as IFN-γ producers when challenged with IL-23 *in vitro* both at long time points (8h, data not shown), and after a short exposure (4 hours, Fig. 3G). Together, our data provide a mechanism for differential function in ILC3 subsets. Whereas IL-22 expression is independent of STAT4 and occurs early during activation, IFN-γ expression in NCR^+ ILC3 is slightly delayed and requires T-BET, STAT4, and associated chromatin changes of regulatory elements.

3 Concluding Remarks

Our study sheds light on a mechanism by which a lymphocyte subset can perceive a single cytokine very differently based on the regulated expression of an LDTF and SDTF (**model in** Supporting information Fig. 4). The mechanism allows for functional plasticity in ILC3, without a global phenotypic transition to a different state, i.e. type 1 ILCs. This property relies on the presence of the LDTF T-BET, which represents the first condition predisposing a subset of ILC3 towards a type 1 response. Subsequently, the type 1 response is amplified by high basal levels of STAT4 induced by T-BET. The coordinated expression of T-BET together with high STAT4 levels allows IL-23 to induce genes associated with both a type 1 response and type 3 response. Most notably, IL-23-induced robust STAT4 phosphorylation leads to an efficient IFN-γ production in NCR^+ ILC3. Our results provide a translational rationale why targeting IL-23 alone could have therapeutic potential for inflammatory bowel disease and colon cancer in which the ILC3/IL-23 axis was reported to play a major role [19] [32]. Similarly, IL-23 targeting therapy would be beneficial in Crohn's disease in which the accumulation of IFN-γ producing ILCs was reported [33]. Most importantly, our findings help explain why targeting IL-23 and IL-17 are not synonymous and have divergent consequences in clinical trials; anti-IL-23 therapies (ustekinumab, guselkumab, tildrakizumab) provided benefit whereas anti-IL-17 therapy (secukinumab) exacerbated inflammation[34].

4 Materials and methods

4.1 Mice

Female C57BL/6J and *Tbx21*$^{-/-}$ mice were purchased from Jackson Laboratory; *STAT4*$^{-/-}$ mice were provided by M Kaplan[35]. All animal studies were performed according to the NIH guidelines for the use and care of live animals and were approved by the Institutional Animal Care and Use Committee of NIAMS and Italian Ministry of Health.

Author Manuscript Author Manuscript Author Manuscript Author Manuscript

4.2 Cell isolation and activation

Cells from the small intestinal lamina propria (siLP) were isolated after incubation of intestine in RPMI with 0.5 mg/ml DNase I and 0.25 mg/ml Liberase TL (Roche), and purification with 40% Percoll[9]. Cells were stimulated in RPMI medium with 10% FCS, 2 mM glutamine, 100 IU/ml penicillin, 0.1 mg/ml streptomycin, 20 mM HEPES buffer (pH 7.2–7.5) (Invitrogen); and 2 mM β-mercaptoethanol (Sigma-Aldrich). Cells were left untreated or stimulated with IL-23 (50–100 ng/ml; R&D Systems) for 30 minutes for evaluation of phosphorylated-STATs; for 4, 8 or 16 hrs (addition of brefeldin A; GolgiPlug; BD, for 4h) for evaluation of cytokine expression. In the colitis model, siLP cells were isolated from mice treated with 3% DSS (MW 36–50kD, 160110, MP Biomedicals) in the drinking water. Weight loss was monitored, and mice were sacrificed at day 7.

4.3 Flow cytometry

Cell surface staining was performed with anti-mouse CCR6 (140706), CD3ε (145–2C11), CD4 (RM4–5), CD16/CD32 (2.4G2), NK1.1 (PK136), NKp46 (29A1.4). Cytofix/Cytoperm Fixation and Permeabilization solution (BD) was used for anti-mouse IFN-γ (XMG1.2), IL-22 (1H8PWSR), CTLA4 (UC10–4B9), RORγt (B2D), and T-BET (eBio4B10) staining. Anti-STAT4 (8), phosphorylated-STAT3 (4/P-STAT3) and phosphorylated-STAT4 (38/p-Stat4) were stained as described[20]. Antibodies were purchased from eBioscience, BioLegend or BD. Samples were acquired using FACSVerse or FACSCanto (BD Biosciences) and analyzed with FlowJo software (Tree Star).

4.4 RNA Sequencing and transcriptomic analysis

Cells were treated with IL-23 (50 ng/ml) or left untreated, for 4h, after sorting using FACSAria III (BD). Cells isolated from siLP were gated on Propidium Iodide $(PI)^{-}CD3\varepsilon^{-}CD19^{-}NKp46^{+}CD127^{+}NK1.1^{-}$ for $NCR^{+}ILC3$; and $PI^{-}CD3\varepsilon^{-}CD19^{-}NKp46^{-}CD127^{+}KLRG1^{-}CD4^{-}$ for $CD4^{-}NCR^{-}$ ILC3. Purity of sorted cells ranges from 95 to 99% post sort. RNA-seq was performed as described previously[36]. Briefly, total RNA was prepared from 50000 cells by using TRIzol (Life Technologies), and processed to generate mRNA-seq libraries using TruSeq SR mRNA sample prep kit (FC-122–1001; Illumina). Libraries were sequenced for 50 cycles (single read) with a HiSeq 2000 or HiSeq 2500 (Illumina). 50-bp reads were mapped onto mouse genome build mm9 using TopHat 2.1.0. Gene expression values (FPKM, fragments per kilobase exon per million mapped reads) were calculated with Cufflinks 2.2.1[37]. Statistical analysis of differentially expressed genes (DEG) were performed with Partek Genomics Suite 6.6. DEG were selected with following criteria: absolute FPKM>10 in at least 1 condition; fold change >4; protein-coding-genes[38] were included in this analysis. Estimated T cell contamination was negligible based on the absence of *Cd5* expression in the dataset. Volcano plot was generated using R 3.0.1 (R Core Team, 2014); heatmap and hierarchical clustering using Morpheus software (Broad Institute); genomic snapshots were generated using IGV software (Broad Institute). Supplemental Table S1 contains FPKM values for expressed genes (FPKM>10).

Author Manuscript Author Manuscript Author Manuscript Author Manuscript

4.5 Statistics.

Unpaired homoscedastic Student's t test was used to quantify statistical deviation between experimental groups. Asterisks denote significant differences ($P < 0.05$).

Supplementary Material

Refer to Web version on PubMed Central for supplementary material.

Acknowledgments

YM contributed to experimental design, performed, analyzed and interpreted all the experiments, and helped to write the manuscript. GSca, BZ, HYS helped with performing experiments. YK, AS and JJOS contributed to the experimental design and data interpretation, made helpful suggestions and helped to write the manuscript. GSci designed, performed, analyzed, and interpreted all the experiments, conceived the project and wrote the manuscript. We thank J Simone, J Lay, K Tinsley (Flow Cytometry Section, NIAMS), G. Gutierrez-Cruz, S. Dell'Orso (NIAMS Sequencing Facility), Sun HW, Brooks SR (Biodata Mining and Discovery Section, NIAMS), and the NIAMS LACU staff for technical support. This work was supported by the Intramural Research Programs of NIAMS (JJOS); Institut Pasteur, PTR 113–17 (GSci and AS); Italian Association for Cancer Research (AIRC) Special Program Molecular and Clinical Oncology-5 per Mille (AS); the JSPS Research Fellowship for Japanese Biomedical and Behavioral Researchers at NIH (YM).

List of abbreviations used:

IFN	interferon
IL	interleukin
ILC	innate lymphoid cell
LDTF	lineage defining transcription factor
NCRs	natural cytotoxicity triggering receptors
NK	natural killer
SDTF	signal dependent transcription factor
STAT	signal transducer and activator of transcription

7 References

1. Spits H. et al., Nat. Rev. Immunol. 2013; 13:145–9. [PubMed: 23348417]
2. Fang D. and Zhu JJ Exp. Med. 2017; 214:1861–1876.
3. Cording S. et al., FEBS Lett. 2014; 588:4176–81. [PubMed: 24681095]
4. Montaldo E. et al., Eur. J. Immunol. 2015; 45:2171–82. [PubMed: 26031799]
5. Satoh-Takayama N. et al., Immunity. 2008; 29:958–70. [PubMed: 19084435]
6. Cella M. et al., Nature. 2009; 457:722–5. [PubMed: 18978771]
7. Luci C. et al., Nat. Immunol. 2009; 10:75–82. [PubMed: 19029904]
8. Sanos SL et al., Nat. Immunol. 2009; 10:83–91. [PubMed: 19029903]
9. Sciumé G. et al., J. Exp. Med. 2012; 209:2331–2338. [PubMed: 23209316]
10. Klose CSN et al., Nature. 2013; 494:261–5. [PubMed: 23334414]
11. Rankin LC et al., Nat. Immunol. 2013; 14:389–95. [PubMed: 23455676]
12. Sciumè G. et al., Front. Immunol. 2017; 8:1579. [PubMed: 29250060]

Author Manuscript Author Manuscript Author Manuscript Author Manuscript

13. De Obaldia ME and Bhandoola A. Annu. Rev. Immunol. 2015; 33:607–42. [PubMed: 25665079]
14. Song C. et al., J. Exp. Med. 2015; 212:1869–82. [PubMed: 26458769]
15. Rankin LC et al., Nat. Immunol. 2016; 17:179–86. [PubMed: 26595889]
16. Sciumè G. et al., Front. Immunol. 2017; 8:1–5. [PubMed: 28149297]
17. Villarino AV et al., J. Exp. Med. 2017; 214:2999–3014. [PubMed: 28916644]
18. Guo X. et al., Immunity. 2014; 40:25–39. [PubMed: 24412612]
19. Buonocore S. et al., Nature. 2010; 464:1371–5. [PubMed: 20393462]
20. Miyagi T. et al., J. Exp. Med. 2007; 204:2383–96. [PubMed: 17846149]
21. Weizman O-E. et al., Cell. 2017; 171:795–808.e12. [PubMed: 29056343]
22. O'Sullivan TE et al., Immunity. 2016; 45:428–41. [PubMed: 27496734]
23. Cella M. et al., Proc. Natl. Acad. Sci. U. S. A. 2010; 107:10961–6. [PubMed: 20534450]
24. Bernink JH et al., Immunity. 2015; 43:146–60. [PubMed: 26187413]
25. Vonarbourg C. et al., Immunity. 2010; 33:736–51. [PubMed: 21093318]
26. Villarino AV et al., Nat. Immunol. 2017; 18:374–384. [PubMed: 28323260]
27. Watford WT et al., Immunol. Rev. 2004; 202:139–56. [PubMed: 15546391]
28. Tong A-J. et al., Cell. 2016; 165:165–179. [PubMed: 26924576]
29. Takatori H. et al., J. Exp. Med. 2009; 206:35–41. [PubMed: 19114665]
30. Cupedo T. et al., Nat. Immunol. 2009; 10:66–74. [PubMed: 19029905]
31. Bezman NA et al., Nat. Immunol. 2012; 13:1000–1009. [PubMed: 22902830]
32. Geremia A. et al., J. Exp. Med. 2011; 208:1127–33. [PubMed: 21576383]
33. Bernink JH et al., Nat. Immunol. 2013; 14:221–9. [PubMed: 23334791]
34. Abraham C. et al., Gastroenterology. 2017; 152:374–388.e4. [PubMed: 27780712]
35. Kaplan MH et al., Nature. 1996; 382:174–7. [PubMed: 8700209]
36. Shih HY et al., Cell. 2016; 165:1120–1133. [PubMed: 27156451]
37. Trapnell C. et al., Nat. Protoc. 2012; 7:562–78. [PubMed: 22383036]
38. Pruitt KD et al., Genome Res. 2009; 19:1316–23. [PubMed: 19498102]

Author Manuscript Author Manuscript Author Manuscript Author Manuscript

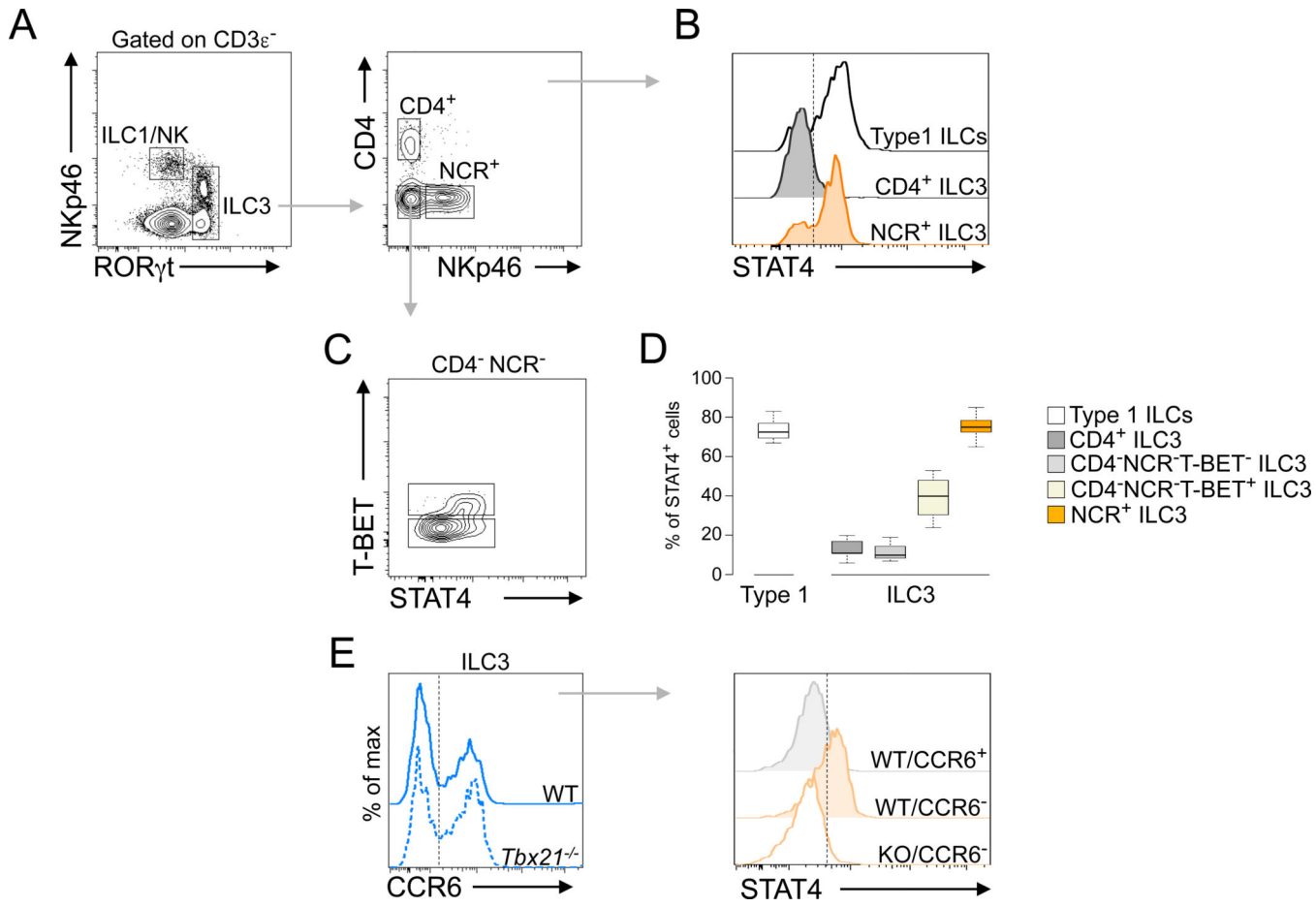

Figure 1. STAT4 is differentially expressed in ILC3.

(A) STAT4 expression was analyzed in ILCs discriminated based on RORγt, NKp46 and CD4 expression. Type 1 ILCs are defined as CD3ε⁻RORγt⁻NKp46⁺ cells; CD3ε⁻RORγt⁺ ILC3 are divided in three populations according to CD4 and NKp46. **(B)** Histogram overlay shows basal STAT4 expression levels in the indicated ILC subsets. A representative experiment of 5 experiments is shown. **(C)** Density plot depicts STAT4 expression relative to T-BET in NCR⁻CD4⁻ ILC3. **(D)** Box plot depicts STAT4 expression in the different ILC subsets; measured as median of the percentage of positive cells, relative to control ($n = 5$). **(E)** STAT4 expression in ILC3 isolated from WT and *Tbx21*$^{-/-}$ mice; ILC3 populations are defined according to CCR6 expression (left panel); histogram overlay shows basal STAT4 expression levels in the indicated ILC subsets (right panel). A representative experiment is shown ($n = 4$; 3 independent experiments were performed).

Author Manuscript Author Manuscript Author Manuscript Author Manuscript

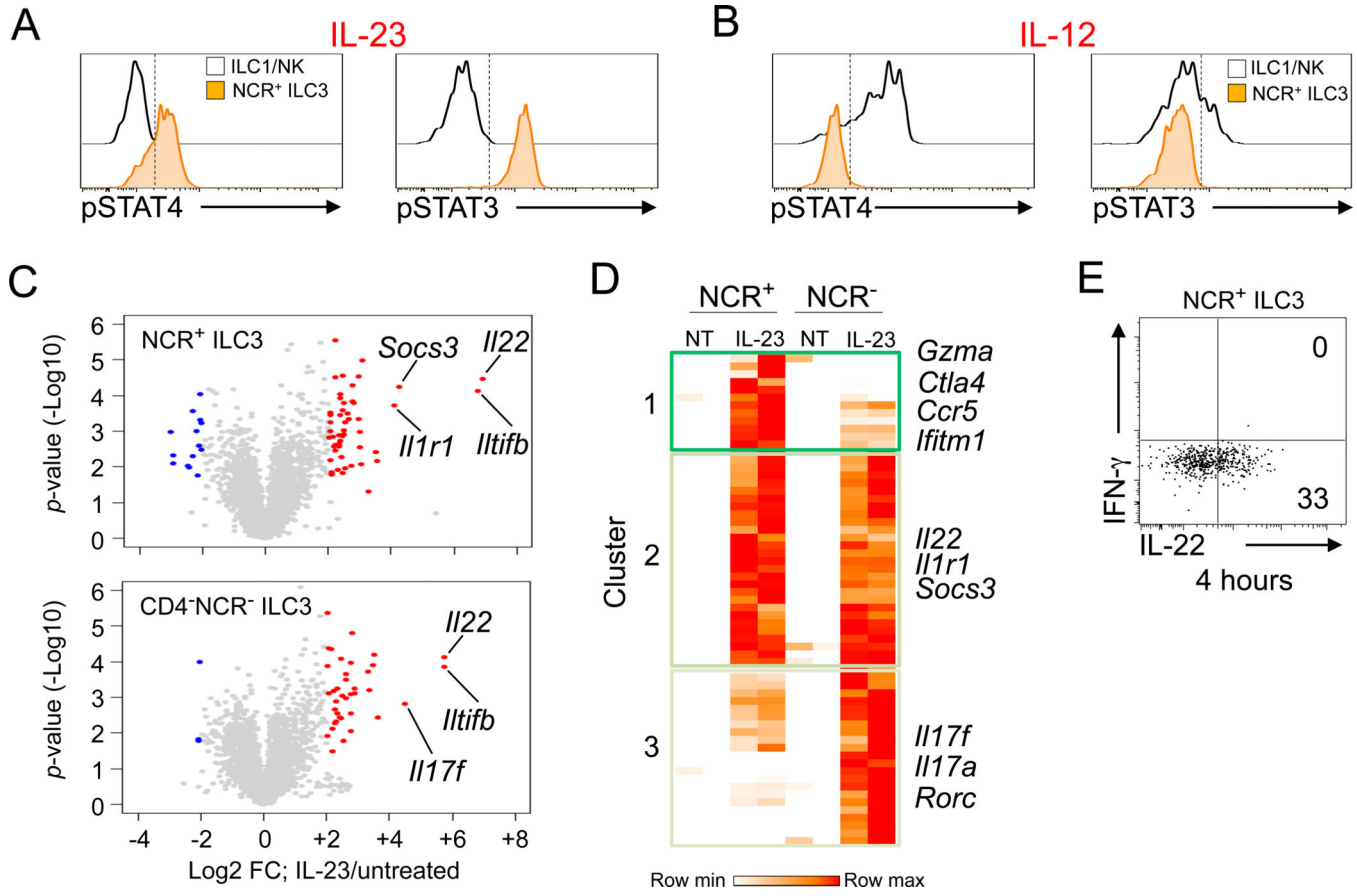

Figure 2. Transcriptomic changes induced by IL-23 in NCR$^+$ ILC3.

(A, B) STAT4 and STAT3 phosphorylation following IL-23 and IL-12 stimulation was performed in NCR$^+$ ILC3 and type 1 ILCs. A representative experiment of 4 experiment performed is shown. **(C)** Volcano plot depicts the transcripts upregulated (red) and downregulated (blue) by IL-23 in NCR$^+$ and CD4$^-$NCR$^-$ ILC3 (4h treatment; FC > 4), see also Supporting information table 2. **(D)** Expression of highly induced transcripts (FC > 4) established in (C) is depicted by heatmap, comparing IL-23 stimulated NCR$^+$ ILC3 and CD4$^-$NCR$^-$ ILC3. Three main subsets are defined based on hierarchical clustering. **(E)** Quadrant plot shows IL-22 and IFN-γ expression in NCR$^+$ ILC3. A representative experiment of 3 performed is shown.

Author Manuscript Author Manuscript Author Manuscript Author Manuscript

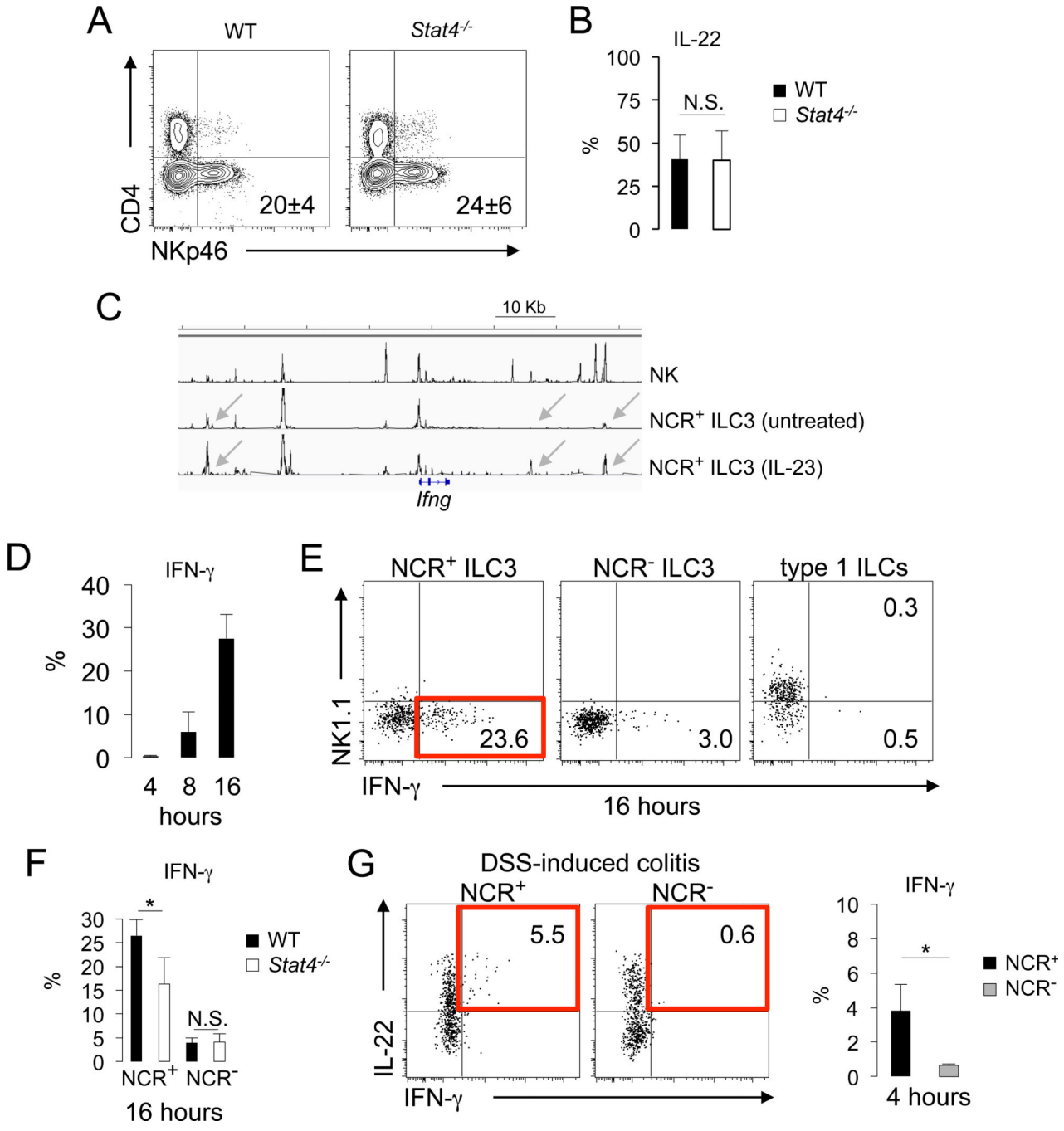

Figure 3. IL-23 drives IFN-γ expression in NCR$^+$ ILC3.

(A) Quadrant plots show CD3ε$^-$ RORγt$^+$ ILC3, dissected based on NKp46 and CD4 expression. Numbers indicate the frequency (mean ± SD) of NCR$^+$ cells, in WT (n=7) and *STAT4*$^{-/-}$ (n=5) mice, among ILC3. A representative experiment of 3 performed is shown. **(B)** Histogram plots depict percentage (mean ± SD) of IL-22$^+$ NCR$^+$ ILC3 after IL-23 stimulation (4h) in WT (black) and *STAT4*$^{-/-}$ (white) mice, (n = 3 per group; 3 independent experiments were performed). **(C)** Genome track view of the *Ifng* locus showing ATAC-seq for ex vivo isolated NK cells, unstimulated and stimulated NCR$^+$ ILC3. **(D)** Histogram plots

Author Manuscript Author Manuscript Author Manuscript Author Manuscript

depict percentage (mean ± SD) of IFN-γ$^+$ NCR$^+$ ILC3 after IL-23 stimulation, at different time points (4, 8, 16h); (*n* = 3 per group; 3 independent experiments were performed). **(E)** Quadrant plots depict IFN-γ production in NCR$^+$ ILC3, CD4$^-$NCR$^-$ ILC3 and type 1 ILCs after IL-23 stimulation (16h) a representative experiment of 3 performed is shown. **(F)** Histogram plots depict percentage (mean ± SD) of IFN-γ$^+$ NCR$^+$ ILC3 and IFN-γ$^+$ NCR$^-$ ILC3 after IL-23 stimulation (16h), in WT (*n* = 3) and *STAT4*$^{-/-}$ mice (n = 4). **(G)** Quadrant plots depict expression of IL-22 and IFN-γ in NCR$^+$ and CD4$^-$NCR$^-$ ILC3 after IL-23 stimulation (4h) in mice (DSS-colitis, day 7). Histogram plots depict percentage (mean ± SD) of IFN-γ$^+$ in NCR$^+$ and CD4$^-$NCR$^-$ ILC3 (*n* = 3, in 2 independent experiments performed). Where indicated asterisks denote significant differences ($P < 0.05$); N.S., not significant.